Composites Part B 148 (2018) 272–280

Contents lists available at ScienceDirect

Composites Part B

journal homepage: www.elsevier.com/locate/compositesb

Nanoscale friction of graphene oxide over glass-fibre and polystyrene

Manoj Tripathi[a,1], Haroon Mahmood[b], David Novel[a,c], Erica Iacob[c], Lia Vanzetti[c], Ruben Bartali[c], Giorgio Speranza[b,c], Alessandro Pegoretti[b,d,**], Nicola Pugno[a,e,f,*]

[a] Laboratory of Bio-Inspired and Graphene Nanomechanics, Department of Civil, Environmental and Mechanical Engineering, University of Trento, via Mesiano 77, I-38123 Trento, Italy
[b] Department of Industrial Engineering, University of Trento, Via Sommarive 9, 38123 Trento, Italy
[c] Centre for Materials and Microsystems, Fondazione Bruno Kessler, via Sommarive 18, I-38123 Trento, Italy
[d] National Interuniversity Consortium of Materials Science and Technology, via G. Giusti 9, Firenze, Italy
[e] School of Engineering and Materials Science, Queen Mary University of London, Mile End Road, E1 4NS London, UK
[f] Ket Lab, Edoardo Amaldi Foundation, Italian Space Agency, Via del Politecnico snc, 00133 Rome, Italy

ARTICLE INFO

Keywords:
Adhesion
Glass fibers
Wear
Thin films

ABSTRACT

Coatings of graphene oxide over two substrates of glass-fibre and polystyrene were obtained by electrophoretic deposition (EPD). A chemical reduction of graphene oxide by exposure to hydrazine hydrate at 100 °C significantly changes the interfacial interaction with the substrate as well as the tribology. Spectroscopic techniques like Fourier transform infrared, Raman spectroscopy, X-ray photoelectron spectroscopy and X-ray diffraction showed that the treatment with hydrazine replaces oxygen functional groups and also induces roughness, a structural disorder and decreases the interlayer separation in the transition from graphene oxide (GO) to reduced graphene oxide (rGO). Treatment with hydrazine reduces adhesion and friction force against diamond like carbon coated Si probe (DLC AFM) at the basal plain of the coatings. Investigation at the edges revealed that the presence of oxygenic functional groups leads to higher shear strength with glass-fibre and polystyrene which reduces after treatment with hydrazine.

1. Introduction

Graphene oxide (GO) is a layered material constituted by graphene sheets functionalized with epoxy and hydroxyl groups [1,2]. The presence of oxygen functional groups makes GO highly dispersible in polar media such as aqueous solutions [3]. This feature of GO is important for the preparation of nanocomposites and superior if compared with CNT, graphene and metallic oxide nanomaterials, since these have a tendency to agglomerate during the synthesis process [3–7]. GO has an amphiphilic character that gives rise to extensive interactions with the polymers. It has been stated that the edge polar groups especially carboxylic of GO might form a chemical bond with the polar polymers, such as hydrogen bonds, while the basal plain groups like phenol hydroxyl and peroxide groups consists of a network of hydrophobic polyaromatic island of unoxidized benzene rings [8] that may induce some physical interlinking such as *C–H, π–π, etc* [9].

Modification of functional groups can tune the surface interactions of GO, useful in a wide range of applications that include sensing and self-healing [10–12]. Numerous results have been reported which prove the possibility to tune the interfacial adhesion between GO and the substrates both with chemical and physical treatments. For instance, pre-treated polyethylene terephthalate (PET) showed prominent adherence to GO film through electrostatic adhesion [1]. Addition of multi-wall carbon nanotubes (MWCNT) and GO can reduce the wear rate by 40% which significantly enhance tribological performances as compared to the MWCNT/epoxy composites. It was observed that GO enhances the MWCNT-epoxy adhesion/interlocking and the glass transition temperature of the composite [13]. GO sheets decorated with nano diamond crystals effectively hindered the aggregation of GO and played a vital role to enhance fracture toughness through crack pinning mechanism in the epoxy polymer matrix composite [14]. Chen et al. [15] modified GO substrate through amino groups to produce covalent bonds between GO and glass-fibre (GF) which enhanced strength and toughness between GF and polymer matrix. Inclusion of GO as an interphase in epoxy/glass composites results in an improved load-transfer between the matrix and the fiber [16].

* Corresponding author. Laboratory of Bio-Inspired and Graphene Nanomechanics, Department of Civil, Environmental and Mechanical Engineering, University of Trento, via Mesiano 77, I-38123 Trento, Italy.
** Corresponding author. Department of Industrial Engineering, University of Trento, Via Sommarive 9, 38123 Trento, Italy.
E-mail addresses: alessandro.pegoretti@unitn.it (A. Pegoretti), nicola.pugno@unitn.it (N. Pugno).
[1] Current affiliation: Department of Mathematics and Physical science, University of Sussex, Brighton, UK.

https://doi.org/10.1016/j.compositesb.2018.04.001
Received 26 October 2017; Received in revised form 29 March 2018; Accepted 1 April 2018
Available online 06 April 2018
1359-8368/

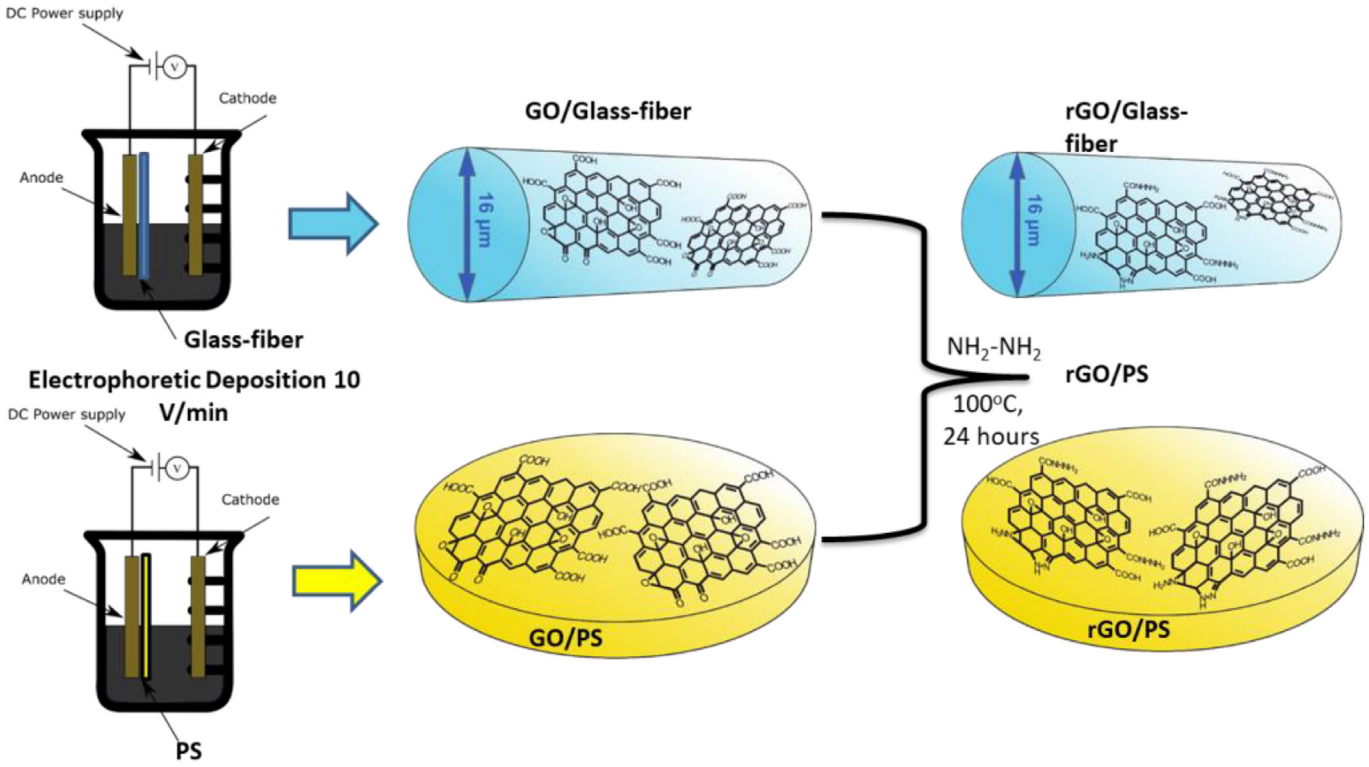

Fig. 1. Schematic representation of the preparation of GO/GF and GO/PS through electrophoretic deposition. The deposition was carried out over cylindrical shape GF nearly 16 µm diameter and flat PS surface. In the subsequent stage, treatment with hydrazine at 100 °C was performed for 24 h.

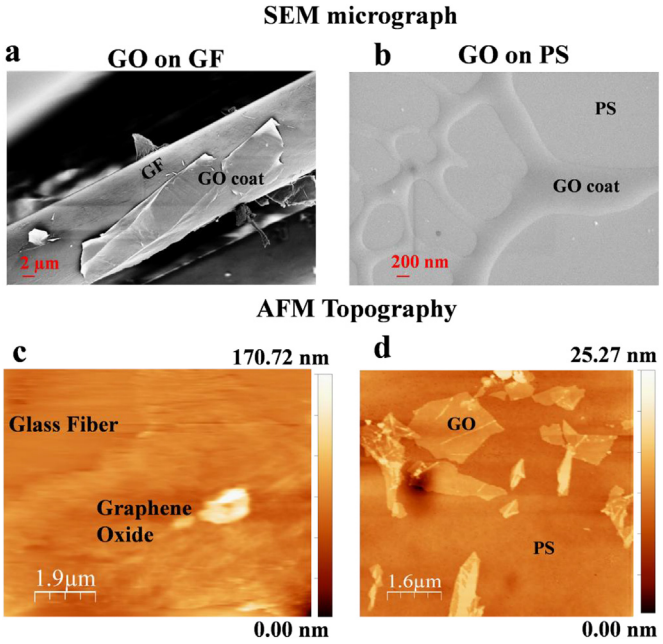

Fig. 2. (a, b) FESEM micrograph of GO on glass-fibre and (b) over polystyrene surface. (c, d) AFM topographic images of the partly covered region of GO over GF and PS respectively. The deposition of GO flakes was significantly influenced by the cylindrical geometry of the glass fibre and flat polystyrene surface showing corresponding curvature and roughness.

The investigation of GO-substrate interfacial interaction is advantageous to evaluate interfacial adhesion between graphene-based fillers, fibers, and polymer matrix [17]. In fact, the mechanical performances of structural composites markedly depend on the way the load is transferred from the matrix to the load-bearing reinforcements [16,18,19], especially with the involvement of shear stresses [20]. Several reports revealed that functionalized GO can provide a mechanical reinforcement in polymer composites higher than graphene [21,22]. Well dispersed GO sheets effectively modify the surface energy and can improve the wettability between fiber and matrix to inhibit crack propagation in the final composite [23]. Good interfacial interaction is essential to ensure efficient load transfer from polymer matrix to the fillers, which helps to reduce stress concentration and improve overall mechanical properties [24]. The GF/epoxy composite display strong hydrogen bonds between GO and GF/epoxy [24]. The polar groups in GO are helpful in enhancing the interfacial adhesion by establishing physical-chemical bonding [7]. Feng et al. [25] found that GO sheets functionalized with polystyrene (PS) chains are able to play a positive effect on the thermal and mechanical properties of the PS related composite. Similarly, the strong interfacial interaction between GO and poly (methyl methacrylate) (PMMA) yields ductile and tougher composites than the pristine PMMA [22].

Several studies indicate that the interaction between GO and substrate is a critical parameter to govern the mechanics of load transfer in polymer composites as well as for the stability of coatings [26]. In this scenario, shear strength (τ) measurement is one of the viable options for the assessment of interfacial adhesion between film and substrate. It is a measurement of the resistance against shear loading of the coating-substrate interface (adhesive strength) or the strength of the coating itself (cohesive strength) [27]. Despite its significance, experimental measurements of the shear strength for GO over polymer substrates have rarely been reported. One of the prime reasons for their scarcity is the interfacial behaviour of GO which is intricately associated with a variety of functional groups and the presence of topological defects [28]. The variation in functional groups diverges the shear response that leads to a wide range of friction characteristics [29], therefore τ depends on the material chemistry and functional structure which determines the physical properties.

In the present work, GO coatings were deposited over polystyrene and glass fibers substrates. After chemical reduction by hydrazine

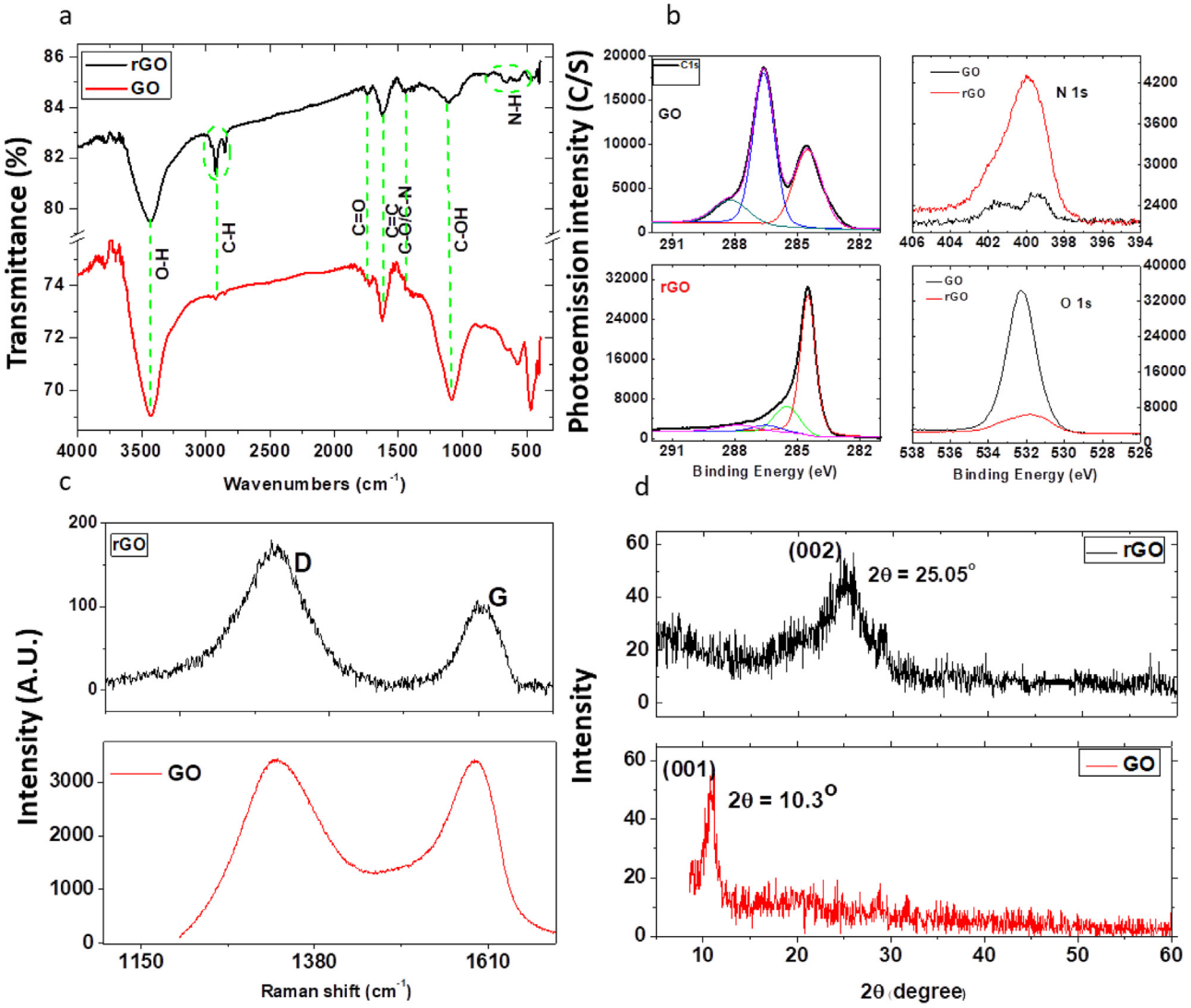

Fig. 3. (a) FTIR of GO and rGO is showing alteration in the functional group after reduction through hydrazine hydrate. (b) XPS spectra of carbon C1s and N 1s for GO and rGO showing elimination of oxygenic groups in rGO. (c) Raman spectra of GO and rGO in range 1100–1650 cm^{-1} of Raman shift showing the presence of D and G peaks. (d) XRD spectra of GO and rGO depicts the generation of the peak for 2θ at 10.3° and 25.05° respectively.

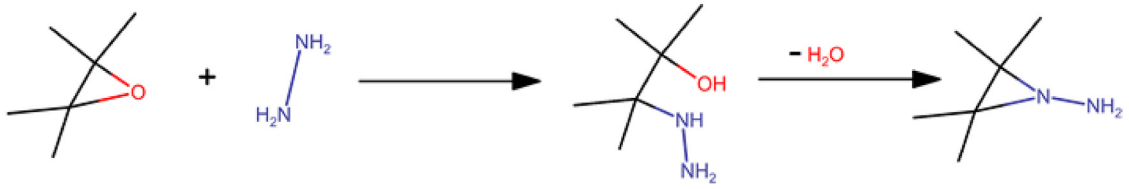

Fig. 4. A proposed reaction pathway for epoxide reduction through hydrazine [41].

Table 1
XPS spectrum data of GO and rGO samples "C(1s)", "O(1s)" and "N(1s)" (wt%).

Sample/(C1s)	C-C/C-H	C-OH	C-O-C	OH-C=O	π-π*
GO	23		34	7.9	
rGO	55.7	15	4.3	5.4	3.3
Sample/(O1s)					
GO	34				
rGO	6.9				
Sample/(N1s)		C=N/C-N	N-H		
GO		0.4	0.6		
rGO		7	2.34		

hydrate they were referred as reduced graphene oxide. The impact of oxygen functional groups and their modification after reduction was analysed through spectroscopic and crystallographic techniques. Adhesion forces and friction response between GO and rGO against AFM (atomic force microscopy) tip was investigated and the shear strength (τ) of GO or rGO coating over GF and PS were evaluated. This aim was reached through tribological studies by atomic force microscopy. The chemical modification significantly changes tribological characteristics of the coated sheets and allows to probe elastic/plastic response of thin films behaviour under compressive and shear stresses.

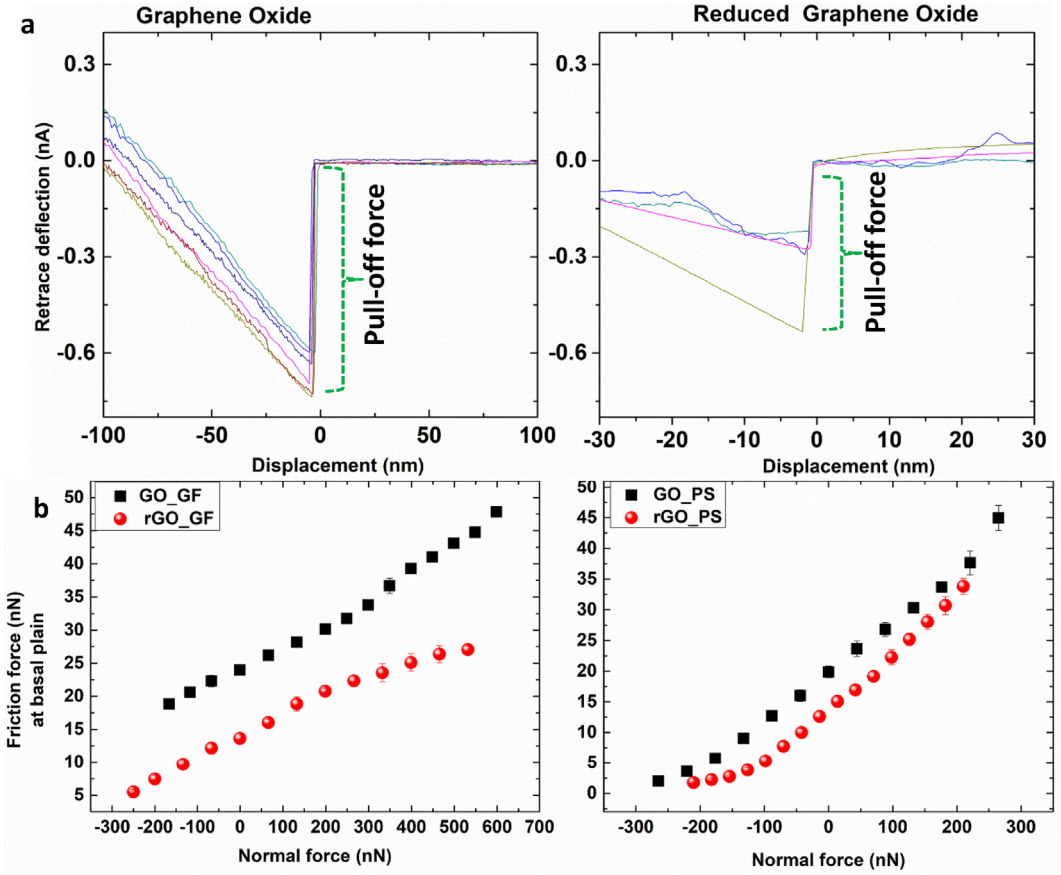

Fig. 5. (a) Pull-off force over GO and rGO against DLC tip apex, the greater pull-off separation represents higher adhesion force between tip apex and surface. The distribution of the pull-off force values is due to use of different cantilevers. (b) Load dependent friction curve for GO and rGO from two different cantilevers showing higher friction values of GO than rGO for both GF and PS surfaces. Most of the cases rGO does not survive for higher load condition that is well sustained by GO.

2. Materials and methods

2.1. Synthesis and coating of graphene oxide over glass-fibre and polystyrene

Graphene oxide was synthesized by following the Hummer's method with slight modification [30]. Briefly, graphite powder (1 g) was added to H_2SO_4 (46 ml) in an ice-cooled bath. This was followed by adding $NaNO_3$ (1 g) and stirring for 15 min. Then $KMnO_4$ (6 g) was slowly added into the mixture to avoid a spontaneous exothermic reaction. The mixture was then stirred for at least 24 h at 35 °C. Finally, an excess of distilled water was added to the above mixture while the temperature was kept at 80 °C. At the end, 30% H_2O_2 was added to the mixture to stop the reaction. The resulting suspension was thoroughly washed using HCl solution and distilled water to remove Mn ions and acid respectively. The obtained brown colour solution was dried in vacuum oven at 50 °C for at least 36 h.

The deposition of GO oxide on GF and PS was performed using the EPD technique as reported elsewhere [16]. In short, a uniform dispersion of GO (1 mg/ml) was obtained by adding GO in deionized water and sonicating it for at least 30 min. This dispersion was used as a bath in which two copper plates were inserted as electrodes. The target to be coated (GF or PS) was placed in front of the anode in such a way that a distance of 2 cm was maintained between the electrode and the target. An applied voltage of 20 V was applied between the electrodes that resulted in the migration of negatively charged GO nanoparticles towards the anode and hence depositing on the target substrate. The deposition was carried out for 5 min. The coated substrates were dried in vacuum at 50 °C for at least 12 h.

For the production of rGO coating on the substrates, the same procedure mentioned above was followed by exposing the coated substrates to hydrazine hydrate for 24 h at 100 °C.

2.2. Synthesis and coating of graphene oxide over polystyrene through spin coating technique

5 wt% solution of polystyrene (M_w ~ 192 kDa, Sigma-Aldrich) in10 ml of N, N dimethylformamide-DMF (Biosyn > 99.9%, Sigma-Aldrich) was prepared and stirred at 50 °C for 2 h. A thin polymer film produced from 10 µl of the resulting polymeric solution deposited on a square silicon wafer with native oxide, having a size of ~ 2 × 2 cm^2. The spin coater (Laurell WS-650) was kept at 500 rpm for 60 s, parameters chosen according to the studies of Hall et al. [31]. In the sequential stage, a solution of 0.2 mg/ml of graphene oxide (few layers of GO flakes, Sigma-Aldrich) in DMF was prepared. The mixture was sonicated by probe sonicator (Hielscher UP400S - H3 sonotrode) to achieve a stable and uniform solution and then centrifuged (Eppendorf, 5417 R) at 14000 rpm for 3 min [32]. The upper layer of supernatant liquid was separated to isolate higher thinner flakes from aggregates and the precipitate. 5 µl of the supernatant were deposited over the PS thin film at 2000 rpm for 60 s to obtain a coating composed of GO. Then, a hybrid system is produced in which PS is sandwich between the silicon wafer and GO. Finally, the sample was heated at 90 °C (Memmert vacuum oven) for 1.5 h under a pressure of 100 mbar to remove the solvent residuals.

2.3. Characterization techniques

The morphology of coated GO over GF was observed using field emission scanning electron microscopy (FESEM) using a Zeiss SUPRA

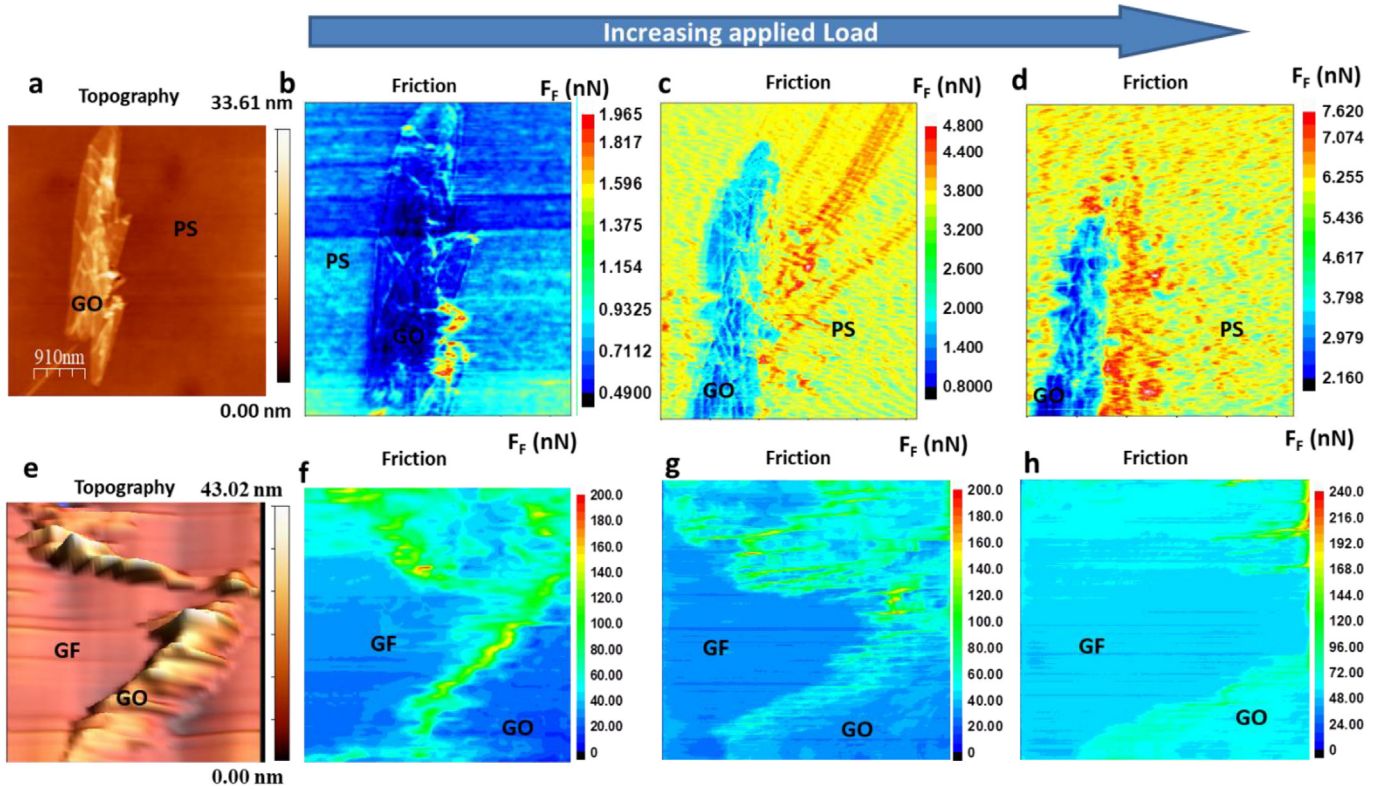

Fig. 6. Friction force map of GO over PS coat and GF with increasing applied load. Panels a and e show topographies of GO over PS and GF surfaces with minimal normal force and their corresponding friction maps are given in panels b and f respectively. The scale bar shows friction force values (nN) for each friction map at fixed normal load. The tribological behaviour of PS and GF are different against DLC coated AFM probe showing higher F_F on PS surface than GO (panel b–c), which is the contrary with respect to GO/GF system (f–h). The increase in normal force leads to wear of the GO edge over both substrates.

40 microscope. For this, approximately 5 nm thick platinum/palladium (80:20) coating was applied prior to the microscopic observation. Thickness (z-direction) and roughness of coated GO were measured by AFM with an NT-MDT solver P47h device operated in intermittent contact mode (tapping mode).

X-ray photoelectron spectroscopy (XPS) analyses were performed using a Kratos Axis Ultra DLD instrument equipped with a hemispherical analyser and a monochromatic Al Kα (1486.6 eV) X-ray source. The emission angle between the axis of the analyser and the sample surface was 90°. For each sample O 1s, C 1s, and N 1s core lines were collected. The quantification reported as a relative elemental percentage was performed using the integrated area of the fitted core lines, after Shirley background subtraction and correcting for the instrument sensitivity factors.

The oxidation level and crystallinity of prepared GO and rGO was evaluated using X-ray diffraction technique by a Rigaku III D-max diffractometer (monochromatic radiation Cu-Kα line with $\lambda = 1.54056$ Å). Measurements were carried out in the 2θ range of 5–80° with a step size of 0.04°.

Raman spectroscopy (Horiba, Jobin-Yvon spectrometer model: Labram, 632.8 nm wavelength, spot diameter ~ 4 μm) was utilised to measure Raman shift (cm^{-1}) of the samples GO and rGO which was carried out in the range of 1000–3000 cm^{-1}.

Fourier transform infrared (FTIR) spectra was carried out at the instrument (model: A Nikolet Avatar 330) with a 4 cm^{-1} resolution. The samples of GO or rGO was mixed individually with potassium bromide (KBr) powder to form a homogeneous mixture and thin disc for analysis was prepared in a compression mold at 10 bar pressure.

Friction force microscopy (FFM) was conducted in contact mode using diamond-like-carbon coated cantilever tip apex (model: DCP01_NTMDT). The measurement was started with an evaluation of the tip radii over silicon test grating "TGT1 from NT-MDT". The line profile of a randomly chosen protrusion (see supplementary, S2) reveals the tip apex radii and its height. The radii of tip apex obtained after deconvolution [33] of line profile given at panel 3 (b) measured ≈ 51 ± 7 nm. The pre-imaging of tip apex using grating before friction measurement is necessary to verify the presence of attached debris after measurement. The calibration of cantilevers used for normal (K_N) and torsional (K_T) force constant was carried out through Sader's method [34,35]. Three cantilevers have been used for the measurement with average value of K_N and K_T are ≈ 6.03 ± 2 N/m and $K_T \approx (8.25 \pm 1) \times 10^{-8}$ N/m respectively.

Friction force and adhesion measurements were carried out on the basal plane of GO/GF, rGO/GF, GO/PS and rGO/PS. The edge of the coatings (GO and rGO) over their corresponding substrate were specifically chosen to measure the shear strength of the coating against (GF and PS). The choice of diamond-like-carbon coated tip for probing is appropriate for tribological operations due to its high stiffness, strength, low chemical reactivity and low adhesion and friction coefficient [36,37]. We did not observe any wear in the tip apex during tribological operations. The delamination of GO was performed in friction mode under the minimal value of the *Gain* associated with feedback look. Otherwise, the cantilever will follow the topography of GO instead of plowing.

3. Results and discussion

3.1. Morphology and chemical characterization

The steps involved in the preparation of GO/GF and GO/PS is showed in a schematic diagram in Fig. 1. The EPD procedure is implemented to coat cylindrically shaped GF of approximate diameter of 16 μm and over flat PS. Prepared coatings were exposed to hydrazine hydrate at 100 °C for 24 h. The comprehensive methodology is

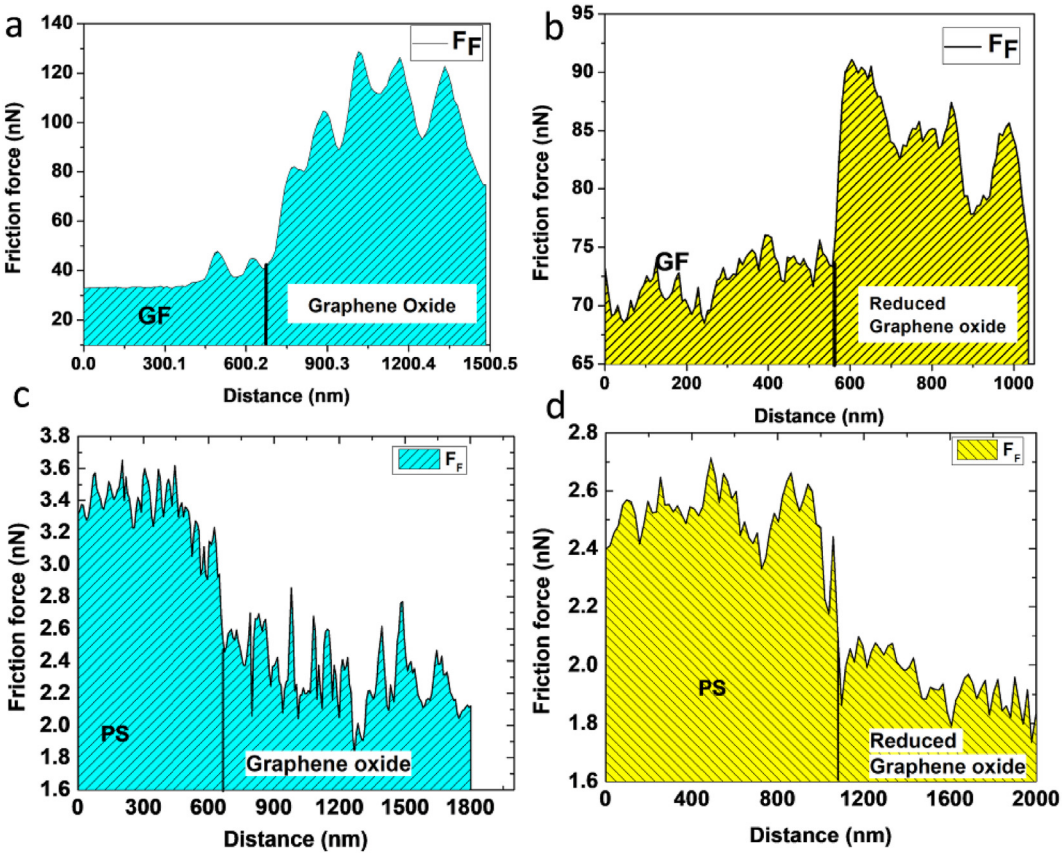

Fig. 7. Friction force (F_F) profile for GO/GF, rGO/GF, GO/PS and rGO/PS at critical applied normal force. The vertical black line separates friction profile over the substrate and their corresponding coatings.

Table 2
Frictional characteristics of GO and rGO for both GF and PS at critical applied normal force. The data are taken from the edge region at the initiation of wear. Where, *P* (pressure applied), γ (shear strain), F_F-F_{sub} (friction force difference between substrate and films) and E_{Diss} (energy dissipated).

Sample	Normal force	Pressure *(P)*	Shear strain *(γ)*	F_F-F_{sub}	(E_{Diss})
	N	N/m^2	radian	N	Nm
GO/GF	3.980E-07	1.94E+07	1.18	1.05E-07	1.0773E-13
rGO/GF	7.41048E-08	3.69E+06	1.19	1.4E-08	1.4364E-14
GO/PS	3.72579E-08	1.85E+06	86	3.2E-09	3.2832E-15
rGO/PS	4.21904E-08	2.10E+06	80	2.2E-09	2.2572E-15

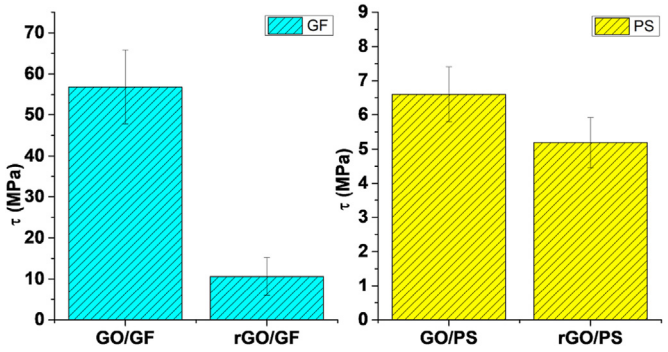

Fig. 8. Distribution of shear strength (τ) of GO and rGO oxide over GF and PS surface.

described in "Method" section. The morphology and distribution of produced GO sheets from EPD procedures are shown in Fig. 2 by FESEM (a, b) and AFM (c, d). GO sheets are wrinkled around cylindrical GF during EPD procedure which leads to the GO film roughness (root mean square, rms = 6.3 nm) and thickness (35 ± 9 nm). Over flat PS surface, GO sheets are thinner (15 ± 3 nm) and possess roughness (rms = 0.48 nm) which is lower by one order of magnitude than in the previous case. The roughness of GO on both surfaces is associated with its heterogeneity due to the presence of functional groups at the edges and basal plain, interfacial adhesion with substrates and the interlayer interactions [38]. We observed a chemical reduction of GO sheets through hydrazine hydrate that increases the nanoscale roughness of the topmost layer of GO/PS (rGO/PS, rms = 0.77 nm) while minor alteration appeared for the rGO/GF, rms = 1.53 nm. It is due to the smoother surface of GO over PS; the impact of hydrazine hydrate is relatively evident (Supplementary S5, S6).

The functional groups at GO and rGO were characterized with different spectroscopic and crystallographic techniques. The qualitative signature of attached functional groups has been investigated through FTIR spectroscopy shown in Fig. 3(a). Reduction through hydrazine hydrate results in an intensification of the peak at 2920 cm^{-1} corresponding to symmetric stretching in -CH_3 and -CH_2- groups [39]. The transmittance peak of the epoxy group is around 1095 cm^{-1} that correspond to C-O stretching and epoxy vibrations at 1050 cm^{-1} [40] which has been decreased for rGO. It shows that peak intensities of the oxygenic groups are suppressed after treatment with hydrazine hydrate with the introduction of N components. The incorporation of nitrogen group through hydrazine proposed by Stankovich et al. [41] on the epoxy group is described in Fig. 4. The treatment with hydrazine can cause the ring opening on the epoxy groups and replacement of oxygen by nitrogen.

XPS spectra carried out in the wide range (0–1300 eV) that includes C 1 S, O1S and N 1s are given in supplementary information, S1. The high-resolution of the corresponding peaks are given in Fig. 3 (b). The C 1s core level spectrum is showing three major features due to the chemical bonding of the oxygen to carbon as indicated by C-O (hydroxyl and epoxy groups), C = O peaks (carbonyl group) at 286.5 eV [42] and 288.2 eV respectively and C-C bond at 284.5 eV binding energy [43]. rGO is showing a significant reduction in oxygenic groups while incrementing in C-C bond, Table 1. Inset, N 1s core level increases up to 7 times after treatment with hydrazine treatment. Spectrum O 1s at a binding energy of 532.3 eV is attributed to oxygen bound to carbon, either as C–O–C in epoxy or C–OH in the hydroxyl group [44] are reduced from 34.2% to 4.3%. Our results reveal the majority of the oxygenic functional groups are replaced and sp^3 -hybridized carbon is converted to sp^2 -hybridized carbon. The higher content of oxygen in carbon compound formed through epoxide and hydroxyl groups or by water intercalation in the interlayer space indicate higher binding energy and consequently higher shear retardant property [29]. The coalescing of the functional group into larger agglomerates connects adjacent GO layers via hydrogen bond network and serves as a primary stiffening agent in the shear response of the GO film. It might explain higher friction signals near edge regions in our friction map, see Fig. 6 in the subsequent section.

Raman spectrum of GO was found to be significantly transformed after the reduction, Fig. 3(c). In the spectra of GO and rGO, two fundamental vibrational peaks are observed at 1331 cm^{-1}, 1597 cm^{-1} corresponding to D and G peaks respectively. The G peak corresponds to vibration of sp^2-hybridized carbon and D peak is due to a structural disorder associated with vacancies and grain boundaries on graphitic surface [45,46]. The ratio I_D/I_G for GO and rGO is 1.1 and 1.6 respectively signifying higher disorder structure due to the replacement of oxygen during reduction procedure through hydrazine hydrate treatment. Increasing the intensity of D peak due to sp^2 carbon cluster indicate the presence of isolated graphene domain in rGO in comparison to GO [47].

XRD spectra of GO at Fig. 3 (d) exhibit basal reflection peak (002) at $2\theta = 10.03$ (c.a. d spacing = 0.88 nm). The increase in d spacing due to the intercalation of water molecules and the formation of oxygen containing functional groups [48]. rGO has a broad peak centered at $2\theta = 25.05^{\circ}$ represent a decrease in d spacing up to 0.36 nm indicate removal of functional group and re-stacking of carbon layers [47]. The stack spacing impacts the strength of the bond between the layers and affects the stiffness and strength of a layered structure [29]. It indicates that chemical reductions with hydrazine hydrate not only affect the surface but also influences the bulk of GO.

3.2. Adhesion and friction force measurement

The friction measurement was carried out by the torsion of the AFM cantilever during tip sliding and adhesion force was measured through pull-off force measurement. The presence of oxygen functional groups in GO increases the adhesion force with respect to rGO, Fig. 5(a). It is measured as 25 ± 2 nN for GO and 13 ± 1 nN for rGO. Load dependent friction shows significant differences in friction between GO and rGO surfaces for both GF and PS substrates. For example, at a fixed normal force of 130 nN GF surface showed shear forces of 28.2 ± 0.3 nN and 18.8 ± 1 nN for GO and rGO respectively; similarly on PS such shear forces were of 29 ± 0.5 nN and 25.2 ± 1 nN for GO and rGO respectively. Several reports revealed that chemical modifications of graphene over a substrate significantly changes their tribological characteristics and mechanical properties [14,49]. The friction force on GO surface is up to 8 times larger than graphene, 3 times for hydrogenated graphene [50] and nearly 6 times for fluorinated graphene [51]. Density functional theory calculations showed GO has a larger energy corrugation and shear strength than graphene [50]. The higher value of adhesion forces and higher shear strength due to attached oxygenic functional groups [52] causes larger friction force values of GO surfaces. It is expected that the presence of epoxide and hydroxyl groups attained through interlayer hydrogen bond, leads to dissipation and hence gives rise to the friction [29]. Nevertheless, controlled reduction of GO or substituting functional groups can be tuned to a certain level. The coefficient of friction (COF) between DLC tip and GO, rGO measured through linear fits are obtained in ranges 0.037 to 0.067 and 0.026 to 0.02 respectively for different cantilvers (from Fig. 5, Figs. S4e and S5f). The values are close to those reported for macroscale friction coefficient (0.05) between steel ball (ball-on-plate tester, radius = 1.5 mm) and 50 nm thick GO. The absolute values of friction and adhesion forces vary with tribo-chemistry between the interfaces. Nevertheless, it is commonly observed for carbon compound that higher contents of the oxygenic group (i.e. lower C/O ratio) increase the friction and adhesion forces [53] while its annihilation leads to lower friction force [50], [43].

The friction force at the edges of coatings are higher than in their basal plain regions due to the presence of structural defects [54], attached functional groups [55] and thickness of vicinal carbon atoms at the edges (see S3). It causes higher density of functional groups simultaneously exposed to sliding probe which leads to higher friction force responsible for the vulnerability of the coat. The increment of normal force coupled with shear forces leads to frequent wear and delamination of the edge regions [56]. We observed mechanical deformation of edges of GO over PS and GF surfaces under applied normal forces, Fig. 6. The significant shear displacement of GO along the scanned region suggests a predominant adhesive failure in applied load range. The values of normal force applied to initiate wear at the edges over GO/PS are 37, 74 and 111 nN respectively, Fig. 6 (a–d, further higher values of normal force are given in supplementary information, S4, a-d) and over GO/GF are 398, 441 and 500 nN respectively, Fig. 6(e–h). For the lower normal loads (37 nN), the friction force is similar for both PS and GO coat. Edges are the regions of higher values of friction force, which makes edges more fragile than basal plain. On the contrary GF has lower friction force than GO surface and initiation of wear achieved at normal force is one order of magnitude higher than GO/PS system. These results evidence a stronger interfacial adhesion between GO-GF than GO-PS. However, friction force decreases significantly after hydrazine treatment of GO for both substrates, Fig. 7. The applied normal force also drop to 74 nN for rGO/GF and 42 nN for rGO/PS for the annihilation of the rGO sheets (supplementary, S5).

Fig. 7 shows friction profiles as a function of displacement by cantilever at critical normal force beyond which permanent deformation has occurred perpendicular to the scan direction. The friction profile illustrates friction characteristics between substrates (GF and PS, separated by a vertical black line) and the coats (GO and rGO). For GO/GF system, the friction force is recorded lower at the substrates (GF) than at the coatings (GO). This condition favors the delamination of the GO and rGO sheets rather than producing a significant wear at the substrate [57]. In GO/PS system, both substrate and coat show comparable friction forces (0.7 nN for GO and 0.8 nN for PS) at lower values of normal force (see Fig. 6(b) and Fig. S4e) but wear has been observed over PS (Fig. S5 g, e, phase contrast) along with removal of GO and rGO. We used friction profile at the edge region as useful sites to interpret shear strength of the coating under critical normal force, Table 2.

The area under the profile of friction force-displacement plot (Fig. 7) is associated with the total energy dissipated (E_{DISS}). Friction force at the plowed region can be de-convoluted into interfacial and plowing components. Friction force (F_F) comprises contribution from the substrates (F_{sub}) and interfacial adhesion between sheets and substrates (GF and PS) (F_{IF}), namely:

$$F_F = F_{IF} + F_{sub} \quad (1)$$

F_F-F_{sub}, remove the contribution from substrates and contains only

interlayer and interfacial adhesion used to measure the shear strength. The measured F_F-F_{sub} is reported in Table 2. The work done by the shear force (F_F-F_{sub}) and the delaminated length is used to evaluate the energy dissipated per unit area (2Γ). The relation between shear strength τ and E_{Diss} is derived by Pugno et al. [58] is as follows:

$$\Gamma = \frac{E_{Diss}}{A} = \frac{1}{2}\frac{(\tau + P\mu)^2 h}{G_a} \quad (2)$$

where A is the area of delamination, G_a is the shear modulus of the interface, P is the pressure applied and h is the thickness of GO coat. The scratch length (l) is measured as 1 μm and the width was 102 nm for all measurements. Assuming the condition of zero applied pressure (i.e. P = 0) in equation (2), shear modulus is calculated as follows:

$$\frac{2\,E_{Diss}}{lbh} = \tau\gamma \quad (3)$$

where γ is the ultimate shear strain and correlates to shear modulus ($G_a \approx \tau/\gamma$) and shear strength of the interface. It is estimated as γ = arctan (y/h) (Table 2); here y is the elastic shear displacement measured from friction profile just before critical condition as described by Hunley and coworkers [59]. Initially, from equation (3), shear modulus at zero applied pressure is calculated. Substituting this value of G_a in equation (2) at applied pressure reported in Table 2 leads shear strength as reported in Fig. 8. The standard deviation is associated with variation of thickness of delaminated GO. The detailed calculation is expressed in our previous work [26]. Our results include dissociation of interlayer interaction as well as interfacial adhesion, therefore, τ is higher than interfacial shear stress (ISS) 5.3 ± 3.2 MPa for GO [28]. We repeated the same procedure for GO and rGO produced from spin coating technique over PS surface shows similar values of shear strength (S6).

4. Conclusion

GO and rGO through hydrated hydrazine were investigated over GF and PS surfaces. The morphological and chemical characterization revealed a significant impact of chemical reduction. The roughness of the coating was found to increase after hydrazine treatment especially on GO/PS due to the involvement of additional hydrazine groups. A substantial amount of oxygenic functional groups of graphene oxide were replaced by hydrazine and resulted in a small quantity of O and N atoms. The interlayer separation has been reduced from 0.88 nm to 0.35 nm indicating removal of intercalated functional groups and restacking of carbon layers. Raman spectra showed an increase in ID/IG for rGO, which implies higher disorder structure due to the replacement of oxygen during chemical reduction. The adhesion force measured through pull-off force is found nearly half than for rGO. It significantly affects the frictional response against AFM tip in which COF was reported to be lower for rGO than for GO. These results have been validated using different DLC coated cantilevers. The edge regions were chosen to measure the shear strength of the coating with their corresponding substrates. The delamination of GO and rGO edges occurred with increasing normal load and the following order relation for τ was observed: GO/GF > rGO/GF > GO/PS > rGO/PS. It shows that GO has higher interfacial interaction in GF and PS, nevertheless its treatment with hydrazine reduces the adherence with the substrate.

Acknowledgement

N.M.P. is supported by the European Commission H2020 under the Graphene Flagship Core 2 No. 785219 (WP14 ″Polymer composites") and under the Fet Proactive "Neurofibres" No. 732344.

Appendix A. Supplementary data

Supplementary data related to this article can be found at http://dx.doi.org/10.1016/j.compositesb.2018.04.001.

References

[1] Gómez-Navarro C, Meyer JC, Sundaram RS, Chuvilin A, Kurasch S, Burghard M, et al. Atomic structure of reduced graphene oxide. Nano Lett 2010;10(4):1144–8.
[2] Park S, Ruoff RS. Chemical methods for the production of graphenes. Nat Nanotechnol 2009;4(4):217–24.
[3] Moon IK, Kim JI, Lee H, Hur K, Kim WC, Lee H. 2D graphene oxide nanosheets as an adhesive over-coating layer for flexible transparent conductive electrodes. Sci Rep 2013;3:1112.
[4] Talò M, Krause B, Pionteck J, Lanzara G, Lacarbonara W. An updated micromechanical model based on morphological characterization of carbon nanotube nanocomposites. Compos B Eng 2017;115:70–8.
[5] Tornabene F, Fantuzzi N, Bacciocchi M. Linear static response of nanocomposite plates and shells reinforced by agglomerated carbon nanotubes. Compos B Eng 2017;115:449–76.
[6] Meng F, Wang H, Huang F, Guo Y, Wang Z, Hui D, et al. Graphene-based microwave absorbing composites: a review and prospective. Compos B Eng 2018;137:260–77.
[7] Yao X, Gao X, Jiang J, Xu C, Deng C, Wang J. Comparison of carbon nanotubes and graphene oxide coated carbon fiber for improving the interfacial properties of carbon fiber/epoxy composites. Compos B Eng 2018;132:170–7.
[8] Kim J, Cote LJ, Kim F, Yuan W, Shull KR, Huang J. Graphene oxide sheets at interfaces. J Am Chem Soc 2010;132(23):8180–6.
[9] Yang J, Feng C, Dai J, Zhang N, Huang T, Wang Y. Compatibilization of immiscible nylon 6/poly (vinylidene fluoride) blends using graphene oxides. Polym Int 2013;62(7):1085–93.
[10] Pegoretti A, Mahmood H, Pedrazzoli D, Kalaitzidou K. Improving fiber/matrix interfacial strength through graphene and graphene-oxide nano platelets. IOP conference series: materials science and engineering. IOP Publishing; 2016. p. 012004.
[11] Dong H, Qi S. Realising the potential of graphene-based materials for biosurfaces - a future perspective. Biosurf Biotribol 2015;1(4):229–48.
[12] Zhang X, Xue X, Yin Q, Jia H, Wang J, Ji Q, et al. Enhanced compatibility and mechanical properties of carboxylated acrylonitrile butadiene rubber/styrene butadiene rubber by using graphene oxide as reinforcing filler. Compos B Eng 2017;111:243–50.
[13] Shen X-J, Pei X-Q, Liu Y, Fu S-Y. Tribological performance of carbon nanotube–graphene oxide hybrid/epoxy composites. Compos B Eng 2014;57:120–5.
[14] Zhang Y, Rhee KY, Park S-J. Nanodiamond nanocluster-decorated graphene oxide/epoxy nanocomposites with enhanced mechanical behavior and thermal stability. Compos B Eng 2017;114:111–20.
[15] Chen J, Zhao D, Jin X, Wang C, Wang D, Ge H. Modifying glass fibers with graphene oxide: towards high-performance polymer composites. Compos Sci Technol 2014;97:41–5.
[16] Mahmood H, Vanzetti L, Bersani M, Pegoretti A. Mechanical properties and strain monitoring of glass-epoxy composites with graphene-coated fibers. Compos Appl Sci Manuf 2018;104:112–23.
[17] Singh V, Joung D, Zhai L, Das S, Khondaker SI, Seal S. Graphene based materials: past, present and future. Prog Mater Sci 2011;56(8):1178–271.
[18] Karger-Kocsis J, Mahmood H, Pegoretti A. Recent advances in fiber/matrix interphase engineering for polymer composites. Prog Mater Sci 2015;73:1–43.
[19] Fantuzzi N, Tornabene F, Bacciocchi M, Dimitri R. Free vibration analysis of arbitrarily shaped Functionally Graded Carbon Nanotube-reinforced plates. Compos B Eng 2017;115:384–408.
[20] Young RJ, Kinloch IA, Gong L, Novoselov KS. The mechanics of graphene nanocomposites: a review. Compos Sci Technol 2012;72(12):1459–76.
[21] Palermo V, Kinloch IA, Ligi S, Pugno NM. Nanoscale mechanics of graphene and graphene oxide in composites: a scientific and technological perspective. Adv Mater 2016;28(29):6232–8.
[22] Goncalves G, Marques PAAP, Barros-Timmons A, Bdkin I, Singh MK, Emami N, et al. Graphene oxide modified with PMMA via ATRP as a reinforcement filler. J Mater Chem 2010;20(44):9927–34.
[23] Rafiee MA, Rafiee J, Srivastava I, Wang Z, Song H, Yu ZZ, et al. Fracture and fatigue in graphene nanocomposites. Small 2010;6(2):179–83.
[24] Zhang X, Fan X, Yan C, Li H, Zhu Y, Li X, et al. Interfacial microstructure and properties of carbon fiber composites modified with graphene oxide. ACS Appl Mater Interfaces 2012:4.
[25] Fang M, Wang K, Lu H, Yang Y, Nutt S. Covalent polymer functionalization of graphene nanosheets and mechanical properties of composites. J Mater Chem 2009;19(38):7098–105.
[26] Mahmood H, Tripathi M, Pugno N, Pegoretti A. Enhancement of interfacial adhesion in glass fiber/epoxy composites by electrophoretic deposition of graphene oxide on glass fibers. Compos Sci Technol 2016;126:149–57.
[27] Kašparová M, Volak J, Zahálka F, Houdková Š. Shear strength of thermally sprayed coatings. Mater Sci Eng 1998;251:166.
[28] Daly M, Cao C, Sun H, Sun Y, Filleter T, Singh CV. Interfacial shear strength of multilayer graphene oxide films. ACS Nano 2016;10(2):1939–47.
[29] Wang L-F, Ma T-B, Hu Y-Z, Wang H. Atomic-scale friction in graphene oxide: an interfacial interaction perspective from first-principles calculations. Phys Rev B 2012;86(12):125436.
[30] Hummers WS, Offeman RE. Preparation of graphitic oxide. J Am Chem Soc 1958;80(6):1339.
[31] Hall DB, Underhill P, Torkelson JM. Spin coating of thin and ultrathin polymer films. Polym Eng Sci 1998;38(12):2039–45.
[32] Becerril HA, Mao J, Liu Z, Stoltenberg RM, Bao Z, Chen Y. Evaluation of solution-

processed reduced graphene oxide films as transparent conductors. ACS Nano 2008;2(3):463–70.
[33] Williams PM, Shakesheff KM, Davies MC, Jackson DE, Roberts CJ, Tendler SJB. Blind reconstruction of scanning probe image data. J Vac Sci Technol B 1996;14(2):1557–62.
[34] Green CP, Lioe H, Cleveland JP, Proksch R, Mulvaney P, Sader JE. Normal and torsional spring constants of atomic force microscope cantilevers. Rev Sci Instrum 2004;75(6):1988.
[35] Sader JE, Chon JWM, Mulvaney P. Calibration of rectangular atomic force microscope cantilevers. Rev Sci Instrum 1999;70(10):3967.
[36] Fletcher PC, Felts JR, Dai Z, Jacobs TD, Zeng H, Lee W, et al. Wear-resistant diamond nanoprobe tips with integrated silicon heater for tip-based nanomanufacturing. ACS Nano 2010;4(6):3338–44.
[37] Sumant AV, Grierson DS, Gerbi JE, Birrell J, Lanke UD, Auciello O, et al. Toward the ultimate tribological interface: surface chemistry and nanotribology of ultrananocrystalline diamond. Adv Mater 2005;17(8):1039–45.
[38] Gao Y, Liu L-Q, Zu S-Z, Peng K, Zhou D, Han B-H, et al. The effect of interlayer adhesion on the mechanical behaviors of macroscopic graphene oxide papers. ACS Nano 2011;5(3):2134–41.
[39] Lambert JB, Shurvell HF, Lightner DA, Cooks RG. Introduction to organic spectroscopy. Macmillan Publishing Company; 1987.
[40] Cano M, Khan U, Sainsbury T, O'Neill A, Wang Z, McGovern IT, et al. Improving the mechanical properties of graphene oxide based materials by covalent attachment of polymer chains. Carbon 2013;52:363–71.
[41] Stankovich S, Dikin DA, Piner RD, Kohlhaas KA, Kleinhammes A, Jia Y, et al. Synthesis of graphene-based nanosheets via chemical reduction of exfoliated graphite oxide. Carbon 2007;45(7):1558–65.
[42] Liang H, Bu Y, Zhang J, Cao Z, Liang A. Graphene oxide film as solid lubricant. ACS Appl Mater Interfaces 2013;5(13):6369–75.
[43] Berman D, Erdemir A, Zinovev AV, Sumant AV. Nanoscale friction properties of graphene and graphene oxide. Diam Relat Mater 2015;54:91–6.
[44] Hueso JL, Espinós JP, Caballero A, Cotrino J, González-Elipe AR. XPS investigation of the reaction of carbon with NO, O2, N2 and H2O plasmas. Carbon 2007;45(1):89–96.
[45] Ferrari AC. Raman spectroscopy of graphene and graphite: disorder, electron–phonon coupling, doping and nonadiabatic effects. Solid State Commun 2007;143(1–2):47–57.
[46] Kudin KN, Ozbas B, Schniepp HC, Prud'homme RK, Aksay IA, Car R. Raman spectra of graphite oxide and functionalized graphene sheets. Nano Lett 2008;8(1):36–41.
[47] Thakur S, Karak N. Green reduction of graphene oxide by aqueous phytoextracts. Carbon 2012;50(14):5331–9.
[48] Paredes JI, Villar-Rodil S, Martínez-Alonso A, Tascón JMD. Graphene oxide dispersions in organic solvents. Langmuir 2008;24(19):10560–4.
[49] Ge X, Zhang Y, Deng F, Cho UR. Effects of silane coupling agents on tribological properties of bentonite/nitrile butadiene rubber composites. Polym Compos 2015;38(11):2347–57.
[50] Byun I-S, Yoon D, Choi JS, Hwang I, Lee DH, Lee MJ, et al. Nanoscale lithography on monolayer graphene using hydrogenation and oxidation. ACS Nano 2011;5(8):6417–24.
[51] Kwon S, Ko J-H, Jeon K-J, Kim Y-H, Park JY. Enhanced nanoscale friction on fluorinated graphene. Nano Lett 2012;12(12):6043–8.
[52] Ko J-H, Kwon S, Byun I-S, Choi J, Park B, Kim Y-H, et al. Nanotribological properties of fluorinated, hydrogenated, and oxidized graphenes. Tribol Lett 2013;50(2):137–44.
[53] Hang C, Tobin F. Effect of structure on the tribology of ultrathin graphene and graphene oxide films. Nanotechnology 2015;26(13):135702.
[54] Hölscher H, Ebeling D, Schwarz UD. Friction at atomic-scale surface steps: experiment and theory. Phys Rev Lett 2008;101(24):246105.
[55] Xiao J, Zhang L, Zhou K, Li J, Xie X, Li Z. Anisotropic friction behaviour of highly oriented pyrolytic graphite. Carbon 2013;65:53–62.
[56] Bhushan B. Scanning probe microscopy in nanoscience and nanotechnology 2. Springer Science & Business Media; 2010.
[57] Lee K, Polycarpou A. Shear strength determination using the nanoscratch technique and its application to thin solid films. J Mater Res 2006;21:2304–13.
[58] Pugno NM, Yin Q, Shi X, Capozza R. A generalization of the Coulomb's friction law: from graphene to macroscale. Meccanica 2013;48(8):1845–51.
[59] Hunley DP, Flynn TJ, Dodson T, Sundararajan A, Boland MJ, Strachan DR. Friction, adhesion, and elasticity of graphene edges. Phys Rev B 2013;87(3):035417.

Supplementary Information

Nanoscale friction of graphene oxide over glass-fibre and polystyrene

Manoj Tripathi[1,], Haroon Mahmood[2], David Novel[1,3], Erica Iacob[3], Lia Vanzetti[3], Ruben Bartali[3], Giorgio Speranza[3], Alessandro Pegoretti[2,4], Nicola Pugno[1,5,6]

[1]Laboratory of Bio-Inspired and Graphene Nanomechanics, Department of Civil, Environmental and Mechanical Engineering, University of Trento, via Mesiano 77, I-38123 Trento, Italy

[2]Department of Industrial Engineering, University of Trento, Via Sommarive 9, 38123 Trento, Italy

[3]Centre for Materials and Microsystems, Fondazione Bruno Kessler, via Sommarive 18, I-38123 Trento, Italy

[4] National Interuniversity Consortium of Materials Science and Technology, via G. Giusti 9, Firenze Italy

[5]School of Engineering and Materials Science, Queen Mary University of London, Mile End Road, E1 4NS London, UK

[6] Ket Lab, Edoardo Amaldi Foundation, Italian Space Agency, Via del Politecnico snc, 00133 Rome, Italy

*Corresponding authors: nicola.pugno@unitn.it, alessandro.pegoretti@unitn.it

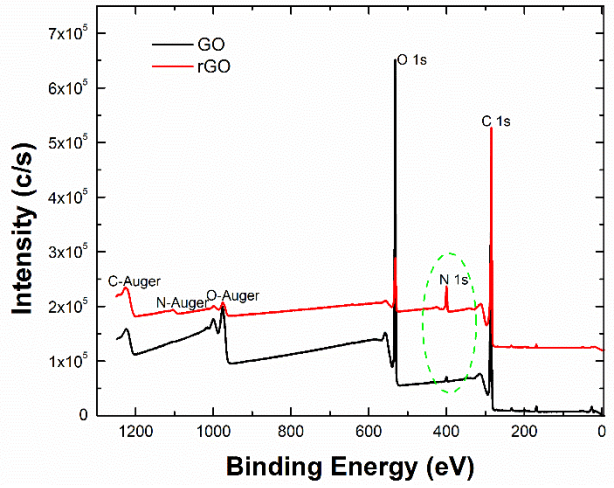

S1: XPS wide scan spectrum of GO and rGO sample. XPS spectra observed at lower BE range (100-600 eV) while Auger transition observed for higher range (900 to 1300eV). The intensity of N peak gets increased in rGO for the both ranges after hydrazine treatment.

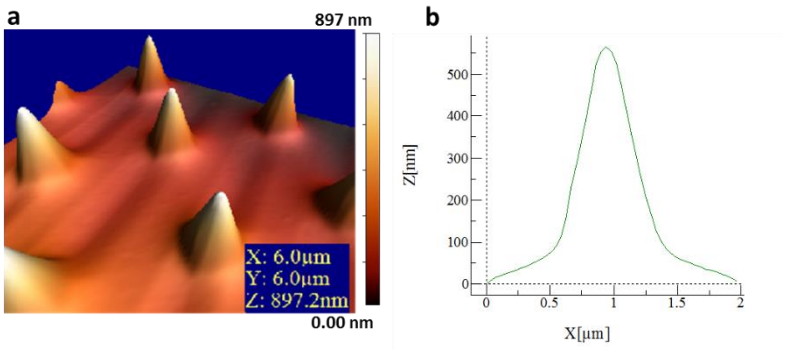

S2: (a) Topographic AFM image of commercial silicon grating (Model no. : TGT1, NT-MDT) to evaluate the shape of diamond coated silica tip apex. (b) The line profile of a protrusion showing the convoluted outline of the tip apex.

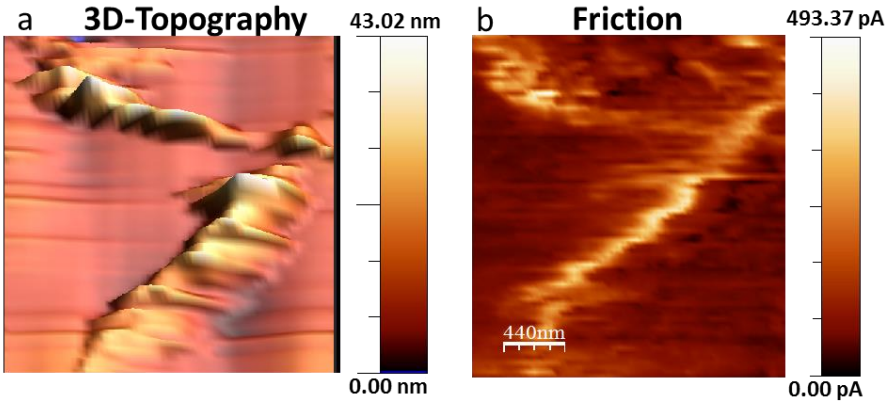

S3: (a) 3-D topography of edge region of GO/GF and panel (b) its corresponding friction map. The intensity of the friction force varies with thickness (43 ± 7) of the edge region. The basal plain has lower friction than edge region.

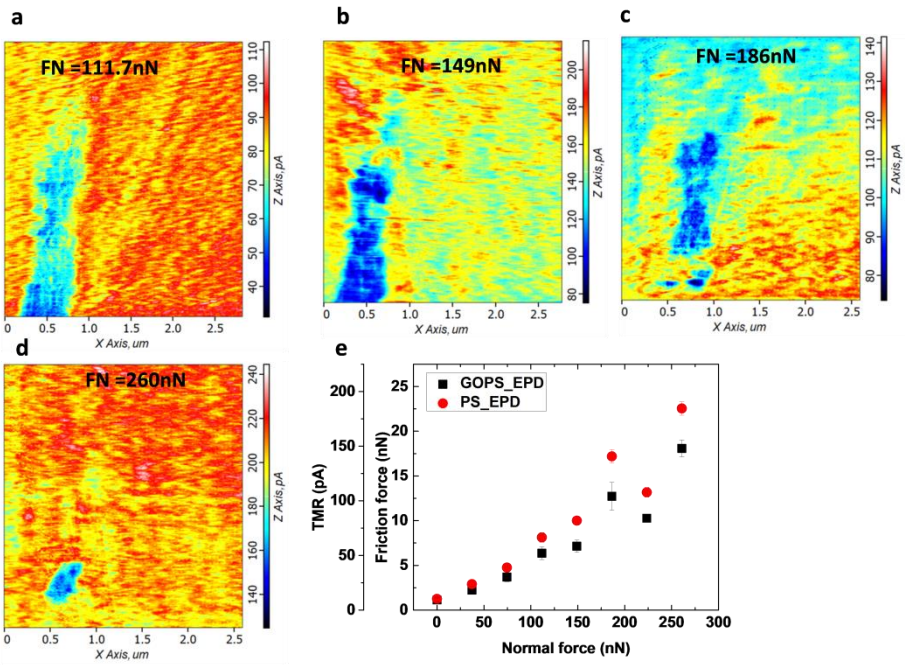

S4: Panel (a-d) showing friction map of GO over polystyrene surface at relatively higher normal force from (111 nN -260 nN). The friction force is increasing with higher applied load for PS region than GO that causes wear at the GO edges. Panel (e) is showing load dependent friction for PS and GO at two different units of (nN) and its corresponding (pA). It is showing the comparable friction force values for both PS and GO at lower values of applied load. The friction force over PS is increasing with applied force than GO showing higher lateral deformation at PS region. The friction curve obtained from same cantilever under single acquisition showing higher friction coefficient of PS as compare to GO.

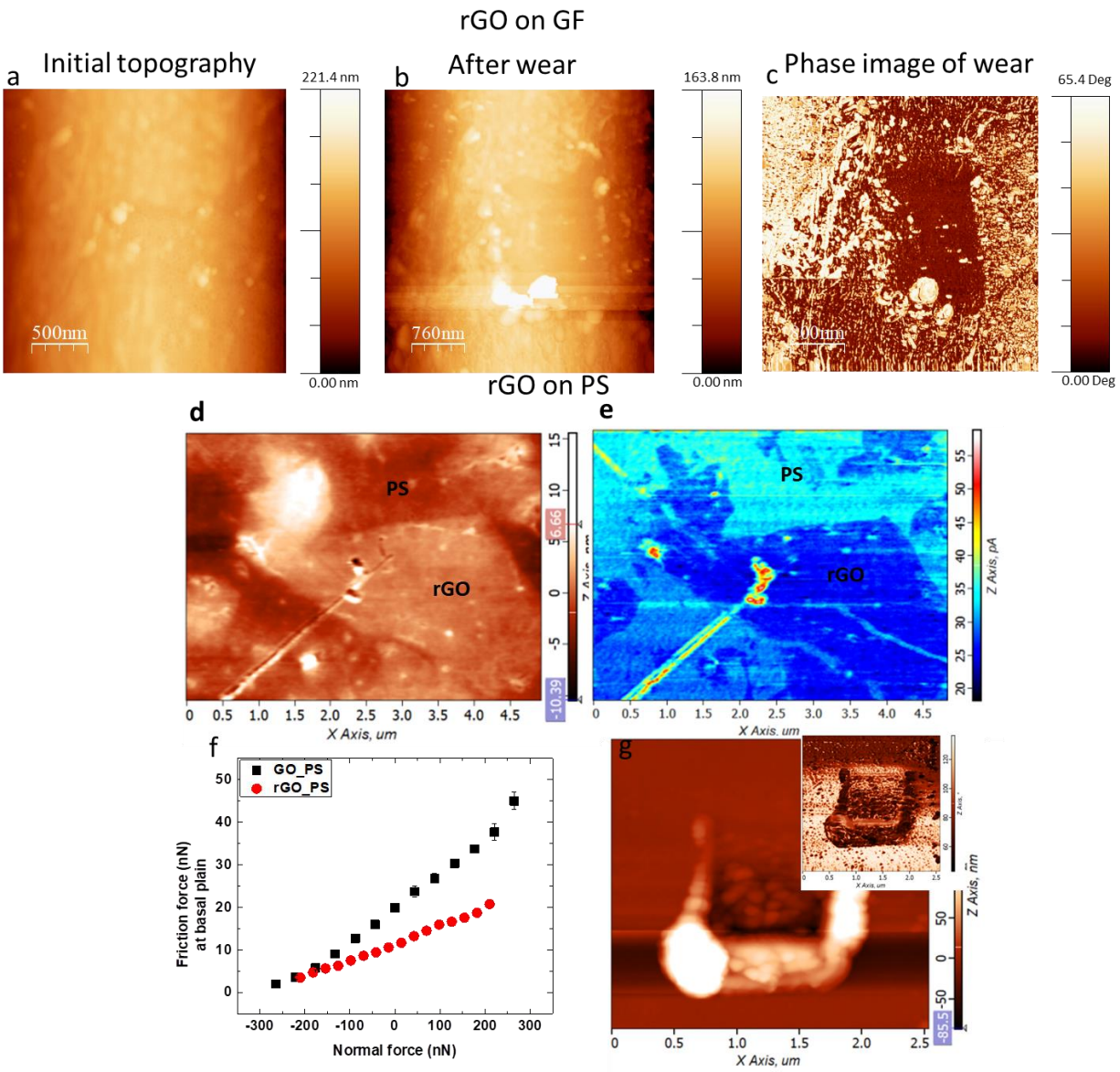

S5: Panel (a –c) showing AFM topographic image of rGO over GF before and after friction measurement. We found nearly 95% removal of rGO during friction measurement as confirmed from its phase contrast image which represent heterogenity, panel (c). The debris collected at the periphery of the frame area shows accumulation of rGO. Panle (d and e) showing topography and friction map of rGO over PS surface. A single scratch line was carried out at zero applied load (note that here adhesion between tip and rGO will induce adhesional force) remove some

portion of rGO. Panel (f) is showing load dependent friction for GO and rGO (using differenet cantilever as used in fig 5 (b)) showing higher friction curve from GO surface that validates the data. Panel (g) showing debris accumulated after FFM measurement. Inset phase contrast showing the effect of applied load on wear of the substrate.

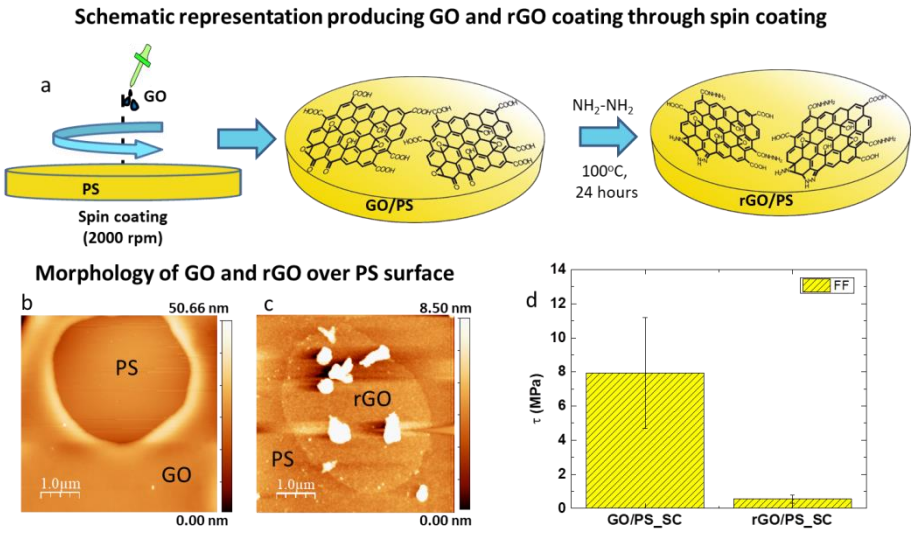

S6: (a) Schematic representation of GO and rGO over PS surface obtained from spin coating technique. Panel (b and c) shows the morphology of the spin coated GO and rGO over the surface of PS carried out by AFM (intermittent contact mode). Reduction with hydrazine can significantly affect the morphology of the surface. The attachment of hydrazine functional group increases the roughness (reported in main text). The bright spots are showing agglomerated GO sheets. The shear strength *(τ)* measured (procedure described in main text) shows higher shear strength of GO over PS surface.